PHYSICAL REVIEW B **88**, 020401(R) (2013)

Frequency dependence of magnetization reversal in thin Fe(100) films

K. Zhernenkov,[1,*] D. Gorkov,[1] B. P. Toperverg,[1,2] and H. Zabel[1]

[1]*Lehrstuhl für Festkörperphysik/Experimentalphysik, Ruhr-Universität Bochum, 44780 Bochum, Germany*

[2]*Petersburg Nuclear Physics Institute, 188300 Gatchina, Russia*

(Received 18 February 2013; revised manuscript received 20 April 2013; published 3 July 2013)

We have studied the magnetization reversal of epitaxial Fe(100) films in an ac magnetic field as a function of frequency between 0.1 and 1.2 MHz by polarized neutron reflectivity. Different modes of magnetization reversal are excited depending on the ac field frequency, those with domain nucleation and propagation, and those with a coherent magnetization rotation. At low frequencies the magnetization follows the external field adiabatically via nucleation and propagation of antiparallel 180° domains. At higher frequencies additional 90° domain walls are being nucleated and propagate. Beyond 0.5 MHz, the magnetization reversal becomes progressively suppressed and finally comes to a stop at about 1 MHz.

DOI: 10.1103/PhysRevB.88.020401 PACS number(s): 75.70.Ak, 75.60.Jk, 75.78.Fg

In magnetic materials relevant time scales range from slow fluctuations of nanoparticles within minutes to microseconds,[1–3] to gyration of vortex cores in micro- to nanoseconds,[4] spin precession on the time scale of picoseconds,[5] up to demagnetization-remagnetization processes within femtoseconds,[6] Among this broad time range the magnetization reversal in thin films and nanostructures is of particular interest as it determines the switching speed of spintronic devices.[7–9] The reversal from one saturated state to the opposite may proceed either via nucleation and propagation of domain walls, or by coherent rotation of the magnetization vector. In practice, the magnetization reversal depends on geometric factors such as film thickness, shape, aspect ratio, and on the angle of the applied magnetic field with respect to the magnetic anisotropy axes.[10,11] Furthermore, in most cases a combination of different processes will actually contribute to a complete reversal cycle.[12]

Driving domain walls (DWs) by an external field, different types of their motion can be distinguished, depending on the field amplitude and temperature.[13] At zero temperature only DW depinning and DW sliding can be excited depending on the field amplitude. At higher temperatures also thermally activated DW creep is possible. DW creep is a slow motion at low fields or in the presence of excessive DW pinning centers and can be disregarded in our present discussion. Another situation occurs at field amplitudes higher than the depinning field or higher than the coercive field in the case of rectangular hysteresis loops. Then the DW motion can be characterized as a viscous sliding with a velocity proportional to the applied field, $v = \mu H$, where μ is the DW mobility.[14] The theoretical prediction of linearity has been confirmed by the observation of domain wall propagation in magnetic nanowires in response to pulse field excitation[16,17] up to the Walker limit,[15] beyond which turbulent and oscillatory motion reduces drastically the sliding velocity. In alternating external fields we expect additional effects to occur, depending on the frequency and amplitude of the ac field amplitude. For small fields domain walls will oscillate in the applied field. At field amplitudes larger than the coercive field and low frequencies magnetization reversal is taking place via nucleation of domains and propagation of DWs.

The magnetization reversal in ac fields or field pulses has been explored to some extent via magnetic susceptibility[18] and magneto-optic Kerr effect (MOKE) measurements.[19,20] These experiments concentrate on measurements of the dynamic complex susceptibility. They yield, however, no information on the frequency dependent magnetization vectors parallel and perpendicular to the applied field. This information is, on the other hand, essential for a complete understanding of the frequency dependent reversal process.

Polarized neutron reflectivity (PNR) provides vector magnetometery similar to vector-MOKE, but measuring magnetization **M** in absolute units with an additional sensitivity to its distribution across the film thickness. This is due to the fact that PNR measures non-spin-flip (NSF) and spin-flip (SF) scattering cross sections, which yield simultaneously two in-plane components via projection of M_y onto the neutron polarization vector and the absolute value $|M_x|$ of the orthogonal magnetization component as a function of depth[21] (for the definition of the coordinate system we refer to the inset of Fig. 1). Up to date, however, the advantages of PNR have not yet been exploited to examine the dynamical characteristics of magnetization reversal processes. In this Rapid Communication we show that all valuable information on the reversal dynamics and kinetics as function of frequency of the field produced by alternating current (ac) applied to the sample can be gained by ac PNR. In particular, ac PNR is well suited for the analysis of various reversal scenarios as this method is highly sensitive to the in-plane magnetization vector and to in-plane domain distribution changing under an ac field within a proper range of frequencies. Here we concentrate on the frequency dependence of the magnetization reversal in an external sinusoidal field of frequencies f up to the MHz regime. This is much higher than frequencies that have been applied so far in MOKE or superconducting quantum interference device (SQUID) experiments.[18–20] ac PNR can clearly distinguish between domain propagation and coherent magnetization rotation, and it can sweep from low frequency viscous motion to high frequencies, where the DW propagation finally comes to a stop. Distinction between these regimes is of considerable interest for characterizing nanomagnetic systems.

Here we present results for a 70 nm thick Fe(100) film epitaxially grown by molecular beam epitaxy (MBE) methods on a 20×20 mm^2 R-plane $Al_2O_3(1\bar{1}02)$ substrate covered with Nb/Cr(100) buffer layers. For details of the MBE growth

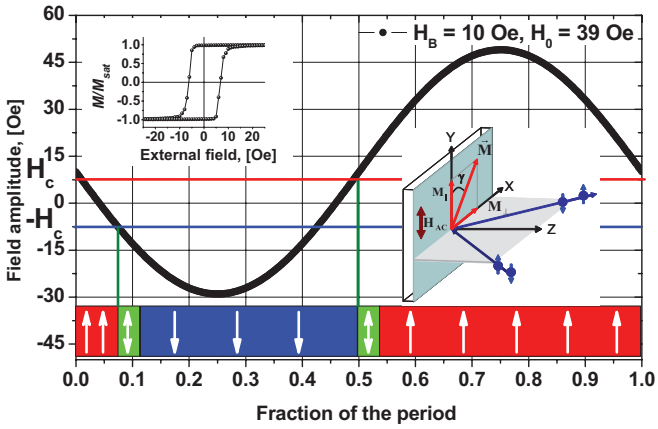

FIG. 1. (Color online) Schematics of the ac field applied to a magnetic sample. $H_{ac}(t) = H_0 \cos(\omega t)$ is the high frequency field applied to the sample, where the center line is offset by the bias field H_b. Whenever $H(t) = H_b + H_{ac}(t)$ crosses the coercive field, the sample magnetization starts to get reversed, as shown schematically in the lower part. The reversal takes place during some transient time τ. The insets top left and bottom right show the hysteresis along the easy axis and the scattering geometry for a monochromatic and polarized incident neutron beam, respectively.

we refer to Ref. 22. The Fe film is protected by FeCr and Cr(100) cap layers. The magnetic hysteresis parallel to the easy axis is sharp and square with a coercive field $H_c \approx 8$ Oe (see the inset of Fig. 1). PNR data were collected with the SuperADAM neutron reflectometer at the Institut Laue-Langevin (Grenoble, France).[23] The [100] easy axis in the film plane was aligned parallel to the X axis displayed within the scattering plane. The other in-plane easy axis [010] was directed along the Y axis normal to the scattering plane. The neutron beam with a wavelength of $\lambda = 0.441$ nm was incident along the X axis and polarized up to 98.5% along the Y axis. The scattering geometry is sketched in the inset of Fig. 1. Two radio frequency (rf) spin flippers and a wide angle solid state analyzer[24] were used to record two NSF ($\mathcal{R}^{++}$ and $\mathcal{R}^{--}$) and two SF ($\mathcal{R}^{+-}$ and $\mathcal{R}^{-+}$) scattering cross sections over the area detector. The sample magnetic environment consists of two coils providing a homogeneous dc-bias field H_b up to 60 Oe and an ac field with amplitudes H_0 up to 120 Oe, both parallel to the Y axis. The rf coil is part of an LC circuit with a frequency f ranging between 0.1 and 2 MHz without noticeable depolarization of the neutron beam. For further details of the ac option we refer to Refs. 25 and 26.

The sample magnetization $M(t)$ evolves under the superposition $H(t) = H_b + H_{ac}(t)$ of dc field H_b and ac field $H_{ac}(t) = H_0 \sin(\omega t)$, with $\omega = 2\pi f$. This is schematically sketched in Fig. 1. Ideally, one can assume that when in the ascending branch of the hysteresis loop the ac field $H_{ac}(t) \geqslant H_c - H_b$, then 180° domain walls nucleate and propagate in the direction perpendicular to the applied field direction. In the descending branch the reversal condition is fulfilled when $H_{ac}(t) \leqslant -(H_c + H_b)$. As a result, the magnetization $M(t)$ should vary periodically between certain limits $M^{min} \geqslant -M_{sat}$ and $M^{max} \leqslant M_{sat}$, where M_{sat} is the saturation magnetization. This variation can, in principle, be recorded with time-resolved (TR) ac PNR (TRAC-PNR). However, for ac frequencies of interest

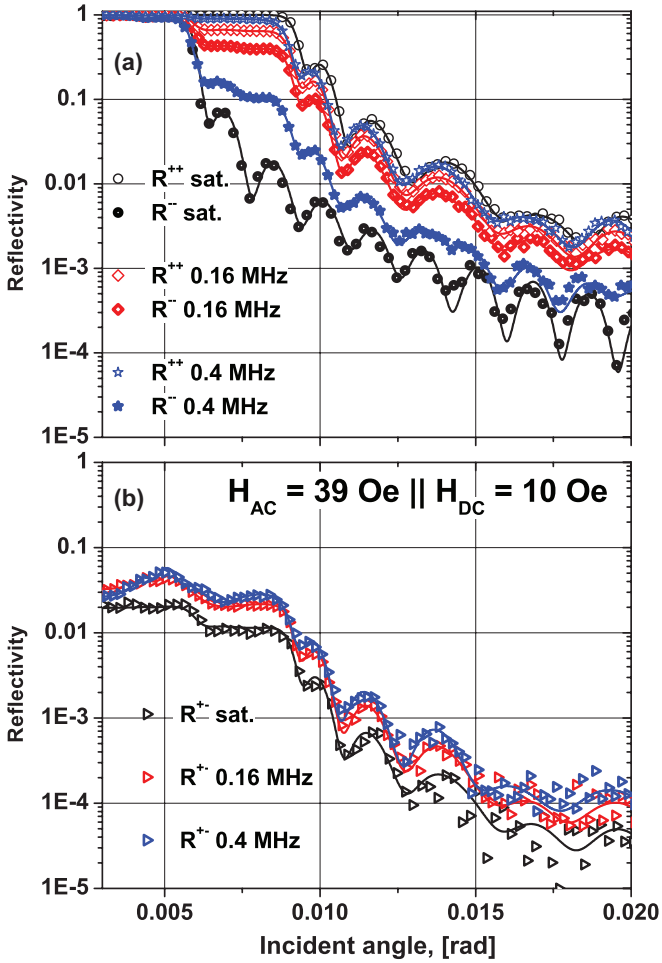

FIG. 2. (Color online) (a) Non-spin-flip reflectivities $\mathcal{R}^{\pm\pm}$ from a 70 nm thick Fe(100) film are plotted as a function of incident angles for different ac magnetic field sweep frequencies with a constant amplitude of 39 Oe applied parallel to the Y axis and parallel to a dc bias field of 10 Oe. The solid lines are least square fits to the data points using the model described in the text. (b) Spin-flip reflectivities $\mathcal{R}^{+-}$ for the same conditions as in (a).

here, TRAC-PNR still faces technical difficulties, which can, in principle, be overcome by employing the modulation of intensity emerging from zero effort (MIEZE) idea,[27] but this is far beyond the scope of the present experiment. On the other hand, the asymmetry set by the bias field can readily be used to retrieve dynamical information without the need for time gating of the PNR signal.

Figure 2(a) shows three pairs of reflectivity curves $\mathcal{R}^{\pm\pm}$ measured at $f = 0.16, 0.4$ MHz and in static saturation plotted against the incident glancing angle. Note that at and above $f = 1$ MHz the reflectivities can hardly be distinguished from saturation curves and are therefore omitted in Fig. 2(a). The static and high frequency case is characterized by NSF PNR, $\mathcal{R}^{++}$ and $\mathcal{R}^{--}$, with well defined critical angles of total reflection for neutron spins parallel or antiparallel to the mean magnetization.[28] In contrast, for intermediate frequencies $f = 0.16$ and 0.4 MHz, the total reflection regime shows both critical angles along each of the NSF reflectivities. These NSF curves can be described by the weighted sum $\mathcal{R}^{\pm\pm} = [(1 \pm \bar{c})|R^+|^2 + (1 \mp \bar{c})|R^-|^2]/2$ of the

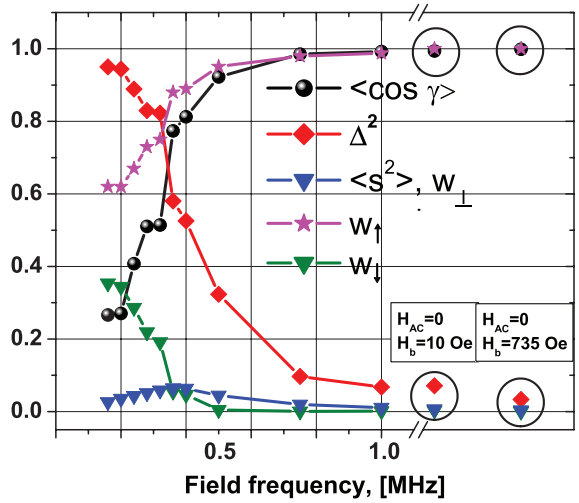

FIG. 3. (Color online) Frequency dependencies of fitting parameters $\bar{c}_\gamma = \langle \cos\gamma \rangle$, $\overline{s^2}_\gamma(f) = w_\perp(f)$, $\Delta^2(f) = \langle \cos^2\gamma \rangle - \langle \cos\gamma \rangle^2$, and weight factors $w_\uparrow(f)$ and $w_\downarrow(f)$. The encircled data points show for comparison the fit parameters in static fields of 10 Oe and saturation field of 735 Oe.

reflection coefficients $|R^\pm|^2$ for neutrons with positive and negative spin projections onto the magnetization direction. The coefficient $\bar{c} = \overline{M(t)}/M_{\rm sat}$ in this equation is determined by the mean magnetization averaged over the ac period $T = 1/f$ and normalized to the saturation magnetization $M_{\rm sat}$. In the case of 180° domains $\bar{c} = w_\uparrow - w_\downarrow$ is determined by the difference between population factors $w_\uparrow$ and $w_\downarrow = 1 - w_\uparrow$ of alternative domain states. Due to the field $H_b \neq 0$ the sample spends more time in the positive field direction than in the negative field direction and $w_\downarrow \neq w_\uparrow$.

For low frequencies f the reversal process, including DW nucleation and propagation, is fully completed within one field cycle. We call this the adiabatic regime, where the domain wall propagation follows the external field. Then the magnetization averaged over the period is determined by the amplitudes of ac and dc fields, and $\bar{c}(f)$ is basically independent of f. This can be seen in Fig. 3 for the first two data points. Above a critical frequency $f_c = f_c(H_0, H_b)$ the magnetization reversal is no longer complete during the ac field cycle and the factor $\bar{c}$ starts to depend on ω. In the limit of very high frequencies the magnetization should finally cease to react on the ac field remaining in saturation. For our samples this limit is reached at $f \sim 1$ MHz. From the dependency $\bar{c} = \bar{c}(\omega)$ one can, in principle, determine the DW velocity and other parameters of magnetization reversal models.[25,26] Here, however, we want to concentrate on more general aspects that permit us to interpret ac PNR data in terms of different magnetization reversal scenarios, and to extract quantitative parameters characteristic for the proportion of domain wall motion versus coherent rotation during reversal.

So far we assumed that 180° DW propagation perpendicular to the polarization axis predominates the magnetization reversal. This is supported by the fact that the NSF reflectivities are strong, whereas the SF reflectivities $\mathcal{R}^{\pm\mp}$ are rather weak. On the other hand, the SF reflectivities cannot be neglected, as shown in Fig. 2(b). They are well above statistical accuracy and SF background due to imperfect polarization and efficiency of its analysis. The effects of the latter are below 2%, as indicated by black symbols in Fig. 2(b). As soon as SF processes cannot be ignored, they signify on the role of magnetization components perpendicular to the polarization vector. These perpendicular components may either be due to partial coherent rotation of the magnetization or propagation of 90° DWs in addition to 180° DWs. These two possibilities should be included into a refined model of the reversal mechanism. In the general noncollinear case the set of reflectivities $\mathcal{R}^{++}$, $\mathcal{R}^{--}$, $\mathcal{R}^{+-}$, and $\mathcal{R}^{-+}$ averaged over the sample surface and ac field period T are customary determined[21] by the set of four equations:

$$\begin{aligned} \mathcal{R}^{\pm\pm} &= \tfrac{1}{4}\langle |(1 \pm \cos\gamma)R^+ + (1 \mp \cos\gamma)R^-|^2 \rangle \\ \mathcal{R}^{+-} &= \mathcal{R}^{-+} = \tfrac{1}{4}\langle |R^+ - R^-|^2 \sin^2\gamma \rangle, \end{aligned} \tag{1}$$

where the averaging runs over all possible angles $\gamma = \gamma(t)$ between the magnetization $\boldsymbol{M}(t)$, and the polarization, $\boldsymbol{P}$ vectors (see the inset in Fig. 1). This averaging is quite simple as soon as the absolute value $|\boldsymbol{M}|$ of domain magnetization is time independent and close to saturation.[29] Then Eq. (1) contains two functions of ω, $\bar{c}_\gamma(f) = \langle \cos\gamma(t) \rangle$ and $\overline{s^2}_\gamma(f) = \langle \sin^2\gamma(t) \rangle$, and two complex reflection amplitudes for $R^\pm$ that depend on the incident angle α. This simple model perfectly fits the NSF and SF reflectivities represented in Fig. 2 with the film structure close to the nominal one, providing two parameters $\bar{c}_\gamma(f)$ and $\overline{s^2}_\gamma(f)$. The frequency dependencies of these parameters are plotted in Fig. 3 along with the mean square dispersion $\Delta^2(f) = \langle \cos^2\gamma \rangle - \langle \cos\gamma \rangle^2$ and other parameters discussed below.

From Fig. 3 it follows that an ac field amplitude $H_0 = 39$ Oe with frequencies below the critical frequency $f_c \leqslant 0.2$ MHz reduces the mean magnetization projection $\langle M_y(f) \rangle / M_{\rm sat} \doteq c_\gamma(f)$ by almost 80% of the saturation value. At the same time the mean squared transverse component $\langle M^2{}_x(f) \rangle / M^2_{\rm sat} = \overline{s^2}_\gamma(f)$ remains relatively small, yielding $\Delta^2(f) \sim 1$. From this we infer that during an ac cycle the magnetization is predominantly (but not solely) reduced by the presence of 180° domains such that $\langle \cos\gamma \rangle \approx 0$, but $\langle \cos^2\gamma \rangle \approx 1$. However, the fact that $\langle M^2{}_x \rangle \neq 0$ indicates either a coherent periodic tilt of the magnetization from the Y axis, or a contribution of domains with magnetization perpendicular to the field. Thanks to the biaxial anisotropy of the Fe film, the latter conjecture appears more plausible at low fields. It is also supported by the large value of $\Delta^2(f) \sim 1$. Then the reversal scenario may involve two types of domains. One of them (80%) is collinear with the Y axis and the remaining one (20%) is oriented parallel to the X axis and perpendicular to the dc field. In fact, 180° domains may more easily nucleate during the reversal when they are framed by low energy 90° DWs, which propagate along the diagonals between two anisotropy axes.

The model with two types of domains can be parametrized by three population factors of domain states for the magnetization along with, $w_\uparrow(f)$, opposite, $w_\downarrow(f)$, and perpendicular, $w_\perp(f) = \overline{s^2}_\gamma(f)$, to the dc field. These factors obey the relationship $w_\uparrow(f) + w_\downarrow(f) + w_\perp(f) = 1$, and their frequency dependencies are plotted in Fig. 3. Interestingly, while the

statistical weight $w_\uparrow(f)$ monotonously increases, and the weight $w_\downarrow(f)$ decreases with frequency, the weight $w_\perp(f)$ (blue triangles) reveal a shallow maximum at $f \approx 0.4$ MHz. At low frequencies $f < 0.4$ MHz the reversal process is clearly dominated by 180° DWs, but at $f \approx 0.4$ MHz the weight $w_\downarrow \approx w_\perp(f)$ and domains with perpendicular magnetization prevail at $f \geqslant 0.4$ MHz. This implies that the nucleation time is longer, and/or mobility is lower for 180° DWs than for 90° DW.

Above $f \geqslant 0.5$ MHz both factors $w_\downarrow \ll 1$ and $w_\perp \ll 1$ become small. Therefore it is not easy to judge whether the reduction of $\Delta^2(f) \ll 1$ indicates a crossover to the magnetization tilt dynamics, when $\langle \cos^2 \gamma(t) \rangle = \langle \cos \gamma(t) \rangle^2$ and $\Delta = 0$. The role of tilt versus 90° domains needs to be explored further by application of an ac field parallel to the X axis while keeping the bias field in the Y direction. Nevertheless from the present results we can conclude that for longitudinal reversal with the ac field applied parallel to the Y axis with increasing frequency the domain wall nucleation and propagation can no longer follow the external field reversal rate. This leads to a freezing of the magnetization direction at frequencies of about 1 MHz. For comparison two data sets (encircled) are shown in Fig. 3 for ac fields switched off and for a dc field of 10 Oe, which is just above coercivity ($H_c = 8$ Oe), and for saturation at 735 Oe. This shows that at 1 MHz the domain kinetics is frozen corresponding to a dc field of 10 Oe, which is, however, still far from real saturation.

Although the investigated Fe film has a macroscopic lateral extension, the domain dynamics actually occurs on a much smaller length scale. Assuming an average domain wall speed of ~100 m/s,[30] the mean distance that the domain walls propagate at a frequency of 0.1 MHz is roughly 0.5 mm, as confirmed by MOKE microscopy.

From our PNR results a clear picture emerges of the mechanisms that control and finally lead to a saturation of the frequency dependence for the magnetization reversal. Using a thin epitaxial Fe(100) film with the easy axis aligned parallel to a dc bias field and ac field of varying frequency, at low frequencies the magnetization reversal process is dominated by nucleation and propagation of antiparallel 180° domains. At higher frequencies, in addition, 90° DWs are nucleated and propagate, which appear to facilitate the propagation of the 180° DWs. Only when crossing the 0.5 MHz barrier, is the magnetization reversal increasingly inhibited and finally stops at about 1 MHz. This richness of information is owed to the different spin-flip and non-spin-flip cross sections, which simultaneously are determined as a function of frequency. Without measuring time resolved magnetic hysteresis curves, the time averaged PNR results reveal the ensemble average probability of the domain distribution within one cycle. By sweeping the frequency, the adiabatic regime, where the magnetic domain reversal follows the external field, can clearly be distinguished from the frequency regime of highest domain distribution during reversal and the frequency regime where the magnetization reversal can no longer follow the external field reversal. Clearly the details depend on many factors, such as film thickness, interface roughness, bias field, ac field amplitude, and others. However, the present example shows that ac PNR opens a new opportunity for the analysis of the high frequency response of magnetic nano- and heterostructures relevant for spintronic applications.

We would like to thank S. Klimko and A. Devishvili for support during the PNR experiments and J. Podschwadek for help during sample preparation. This work was supported by BMBF under Grant No. 05KN7PC1, which is gratefully acknowledged.

*Current address: SPSMS-MDN, UMR-E CEA/UJF-Grenoble 1, INAC, Grenoble F-38054, France.

[1] J. Bansmann, S. H. Baker, C. Binns, J. A. Blackman, J.-P. Bucher, J. Dorantes-Dávila, V. Dupuis, L. Favre, D. Kechrakos, A. Kleibert, K.-H. Meiwes-Broer, G. M. Pastor, A. Perez, O. Toulemonde, K. N. Trohidou, J. Tuaillon, and Y. Xie, Surf. Sci. Rep. **56**, 189 (2005).

[2] O. Petracic, Superlattices Microstruct. **47**, 569 (2010).

[3] P. F. Bessarab, V. M. Uzdin, and H. Jónsson, Phys. Rev. Lett. **110**, 020604 (2013).

[4] M. Kammerer, M. Weigand, M. Curcic, M. Noske, M. Sproll, A. Vansteenkiste, B. Van Waeyenberge, H. Stoll, G. Woltersdorf, C. H. Back, and G. Schuetz, Nat. Commun. **2**, 279 (2011).

[5] M. Farle, T. Silva, and G. Woltersdorf, in *Magnetic Nanostructures*, edited by H. Zabel and M. Farle, Springer Tracts in Modern Physics, Vol. 246 (Springer, Berlin, 2013), p. 37.

[6] H. A. Dürr, T. Eimüller, H.-J. Elmers, S. Eisebitt, M. Farle, W. Kuch, F. Matthes, M. Martins, H.-Ch. Mertins, P. M. Oppeneer, L. Plucinski, C. M. Schneider, Heiko Wende, W. Wurth, and H. Zabel, IEEE Trans. Magn. **45**, 15 (2009).

[7] S. A. Wolf, D. D. Awschalom, R. A. Buhrman, J. M. Daughton, S. von Molna, M. L. Roukes, A. Y. Chtchelkanova, and D. M. Treger, Science **294**, 1488 (2001).

[8] S. D. Bader, Rev. Mod. Phys. **78**, 1 (2006).

[9] S. S. P. Parkin, M. Hayashi, and L. Thomas, Science **320**, 190 (2008).

[10] R. P. Cowburn, J. Phys. D: Appl. Phys. **33**, R1 (2000).

[11] R. Allenspach, in *Handbook of Magnetism and Advanced Magnetic Materials*, edited by H. Kronmüller and S. Parkin, Vol. 2 (Wiley, New York, 2007), p. 915.

[12] R. Skomski, J. Phys.: Condens. Matter **15**, R841 (2003).

[13] J. C. Slonczewski, J. Appl. Phys. **44**, 1759 (1973).

[14] L. D. Landau and E. M. Lifshitz, Phys. Z. Sowjetunion **8**, 153 (1935).

[15] N. L. Schryer and L. R. Walker, J. Appl. Phys. **45**, 5406 (1974).

[16] G. S. D. Beach, C. Nistor, D. Knutson, M. Tsoi, and J. L. Erskine, Nat. Mater. **4**, 741 (2005).

[17] M. Hayashi, L. Thomas, Y. B. Bazaliy, C. Rettner, R. Moriya, X. Jiang, and S. S. P. Parkin, Phys. Rev. Lett. **96**, 197207 (2006).

[18] W. Kleemann, J. Rhensius, O. Petracic, J. Ferré, J. P. Jamet, and H. Bernas, Phys. Rev. Lett. **99**, 097203 (2007).

[19] T. A. Moore, A. Ionescu, and J. A. C. Bland, J. Appl. Phys. **96**, 6546 (2004).

[20] M. Kataja and S. van Dijken, Rev. Sci. Instrum. **82**, 103901 (2011).

[21] H. Zabel, K. Theis-Bröhl, and B. P. Toperverg, in *Handbook of Magnetism and Advanced Magnetic Materials*, edited by H. Kronmüller and S. S. P. Parkin, Vol. 3 (Wiley, New York, 2007), p. 1237.

[22] K. Theis-Bröhl, I. Zoller, P. Bödeker, T. Schmitte, H. Zabel, L. Brendel, M. Belzer, and D. E. Wolf, Phys. Rev. B **57**, 4747 (1998).

[23] A. Devishvili, K. Zhernenkov, A. J. C. Dennison, B. P. Toperverg, M. Wolff, B. Hjörvarsson, and H. Zabel, Rev. Sci. Instrum. **84**, 025112 (2013).

[24] V. Syromyatnikov, A. Schebetov, D. Lott, A. Bulkin, N. Pleshanov, and V. Pusenkov, Nucl. Instrum. Methods **634**, 1 (2011).

[25] K. Zhernenkov, S. Klimko, B. P. Toperverg, and H. Zabel, J. Phys.: Conf. Ser. **211**, 012016 (2010).

[26] S. Klimko, K. Zhernenkov, B. P. Toperverg, and H. Zabel, Rev. Sci. Instrum. **81**, 103303 (2010).

[27] R. Gähler, R. Golub, and T. Keller, Physica B **180-181**, 899 (1992).

[28] Critical angles are determined by nuclear and magnetic optical potentials, while the latter is proportional to the magnetization with a known proportionality coefficient (Ref. 21).

[29] It is also assumed that the average domain size is bigger than the neutron coherence length (Ref. 21). This assumption follows from the fact that off-specular scattering recorded in this set of experiments is quite weak.

[30] T. Ono, H. Miyajima, K. Shigeto, K. Mibu, N. Hosoito, and T. Shinjo, Science **284**, 468 (1999).